Atmospheric Environment 361 (2025) 121514

Contents lists available at ScienceDirect

Atmospheric Environment

journal homepage: www.elsevier.com/locate/atmosenv

Vertical distribution, optical properties, and source attribution of summer dust in southern Tajikistan: ground-based observations and model results

Zhongwei Huang [a,b], Qingqing Dong [a], Tian Zhou [a,b,*], Jianrong Bi [a,b], Rui Chen [c,d], Qiantao Liu [a], Sabur F. Abdullaev [e], Dilovar Nozirov [e], Khan Alam [f], Tianhe Wang [a,b], Wuren Li [b], Ze Li [b], Xiaodong Song [b], Wentao Liu [b]

[a] Key Laboratory of Semi-Arid Climate Changes with the Ministry of Education, College of Atmospheric Sciences, Lanzhou University, Lanzhou, 730000, China
[b] Collaborative Innovation Center for Western Ecological Safety, Lanzhou University, Lanzhou, 730000, China
[c] North Sky-Dome Information Technology(Xi'an)CO., LTD, Xi'an, 710100, China
[d] Xi'an Electronic Engineering Research Institute, Xi'an, 710100, China
[e] Physical-Technical Institute, Academy of Sciences of Republic of Tajikistan, Dushanbe, 734063, Tajikistan
[f] Department of Physics, University of Peshawar, Peshawar, 25120, Pakistan

HIGHLIGHTS

- First lidar measurement of summer dust evolution in southern Tajikistan.
- Persistent elevated dust layers & strong near-surface loading frequently observed.
- Optical differences between dust layers due to sources from complex terrain/flow.

ARTICLE INFO

Keywords:
Lidar
Dust
Southern Tajikistan

ABSTRACT

It is known that dust storms frequently occur during the summer in southern Tajikistan, mainly from satellite-based observations. However, a comprehensive understanding of dust characteristics remains limited due to the scarcity of continuous ground-based measurements. In June of 2023, we established an observational station for investigating the physical and optical properties of dust aerosols in Shaartuz, southern Tajikistan. This study reports dust storms that occurred from July 19 to 26, 2023, focusing on the spatiotemporal distribution and sources of dust aerosols. It is shown that both number and mass concentrations of particles exceeding 10 μm remained substantial throughout the observation period, confirming the persistent presence of coarse-mode dust particles. During the event, PM_{10} and $PM_{2.5}$ concentrations near the ground reached up to 3841 μg/m^3 and 695 μg/m^3, respectively, coinciding with the dust storm outbreak on July 19. Two coexisting distinct dust layers were found based on statistical analysis of lidar-derived depolarization ratio and color ratio. The lower layer, located below approximately 1.6 km, was predominantly impacted by air masses from northwest Central Asia, whereas the higher elevated layer distributed between 2.2 km and 4 km, was originated from the southern desert regions. Moreover, optical properties of these two dust layers are largely different, indicating that impact of dust aerosols originated from various dust sources on climate in southern Tajikistan may complex. These results highlight the characteristics of the spatiotemporal evolution, transport pathways of dust aerosols, helping to further evaluate their climatic and environmental impacts in southern Tajikistan. These results highlight the characteristics of the spatiotemporal evolution and transport pathways of dust aerosols, and help to further evaluate their climatic and environmental impacts in southern Tajikistan.

* Corresponding author. Key Laboratory of Semi-Arid Climate Changes with the Ministry of Education, College of Atmospheric Sciences, Lanzhou University, Lanzhou, 730000, China.
E-mail address: zhoutian@lzu.edu.cn (T. Zhou).

https://doi.org/10.1016/j.atmosenv.2025.121514
Received 1 July 2025; Received in revised form 25 August 2025; Accepted 28 August 2025
Available online 28 August 2025

1. Introduction

Dust aerosols, which are recognized as the most prevalent type of aerosol in the atmosphere, play a crucial role in impacting the Earth-atmosphere radiation balance. They achieve this by absorbing and scattering solar radiation, and they also exert indirect impacts on regional and global climates through cloud microphysical processes (Chen et al., 2023; Ramanathan et al., 2001; Tegen et al., 1996; Toll et al., 2019). Central Asia is identified as one of the primary sources of dust on a global scale (Chen et al., 2020; Liu et al., 2023), characterized by frequent and severe dust storms that contribute approximately 17–20 % of global dust emissions (Indoitu et al., 2012, 2015; Shi et al., 2020). The radiative forcing of dust on both regional and global scales is closely associated with the heights of the dust layer (Li et al., 2025). Therefore, detailed information regarding the vertical distribution of dust is essential for reducing the uncertainty in quantifying the aerosol radiation budget.

Various methods, including aircraft, unmanned aerial vehicles, and tethered balloons equipped with in situ and remote sensing instruments, can be utilized to evaluate the vertical distribution of dust aerosols. However, these techniques are limited by their temporal resolution (Zhou et al., 2023). Satellite observations are similarly restricted by their orbital trajectories, which hinder continuous monitoring of the same location (Shao et al., 2011). Ground-based lidar has emerged as a widely employed instrument for observing the vertical distribution of dust aerosols (Sugimoto et al., 2012; Zhou et al., 2024). Its high temporal and vertical resolution enable it to effectively capture the complex structure of atmospheric feature layers, such as dust layers. Additionally, lidar offers the advantages of facilitating long-term continuous observation of vertical profiles at fixed locations (Dong et al., 2022; Huang et al., 2023b). The acquisition of vertical distribution characteristics of aerosols can contribute to a comprehensive database that helps to study the detailed evolution processes of dust events (Bohlmann et al., 2023; Zhou et al., 2021).

It is indicated that the global average surface dust concentration for the year 2023 was lower than that recorded in 2022 (World Meteorological Organization (WMO), 2024). However, the dust concentration increased in hotspots like Central Asia (Rahnama et al., 2022). Tajikistan, situated in the high mountainous region of Central Asia, possesses a complex and diverse topography that significantly impacts both regional and global climate and ecology (Zhou et al., 2019). Its geographical positioning within an arid and semi-arid region, characterized by a dry climate and low precipitation levels, has led to an increased frequency and intensity of dust storms. These storms predominantly occur from spring to autumn, with the highest frequency observed during the summer months, which coincide with the active period of the adjacent deserts (Papagiannis et al., 2024). As a critical area impacting the synoptic conditions in upstream China, ecological and climatic changes in Central Asia are likely to have substantial implications for regional climate change in Northwest China (Ren et al., 2022).

The severe lack of observational data in Tajikistan and the broader Central Asian region has resulted in current studies failing to provide a comprehensive understanding of dust aerosols in this area (Chen et al., 2022; Rupakheti et al., 2020a). In particular, there is a significant deficiency in knowledge regarding the vertical distribution and optical properties of dust in the southern valley of Tajikistan. In June 2023, an observation station was established in Shaartuz, Southern Tajikistan. The high-resolution vertical profile dataset, in addition to near-surface and column properties of aerosols, presents valuable opportunities for advancing the study of regional climate and environmental conditions (Huang, et al., 2023; Liu et al., 2024).

This study aims to investigate, for the first time, the physical and optical properties, vertical distribution, and sources of summer dust aerosols at the Shaartuz Station during a persistent dust event that occurred from July 19 to July 26, 2023. In Section 2, the data and methods are described, including an overview of the study site, the instruments and the datasets. Section 3 presents the results and discussion, emphasizing the comprehensive observations and potential sources of dust. A summary is provided in Section 4.

2. Data and methods

2.1. Observational station

In Fig. 1, the Shaartuz Station is situated in Ayvadj Meteorological Station in Shaartuz district Khatlon Province, Tajikistan (68.0°E, 36.9°N, 274 m above sea level). The station is located within the Amu Darya Basin and is flanked by high mountains on three sides. It is equipped with advanced instruments such as lidar, sun-sky-lunar photometer, and microwave radiometer, which can provide comprehensive atmospheric observation data. Tajikistan experiences a dry continental climate and is in proximity to several significant dust sources, including the Kyzylkum Desert, Karakum Desert, and Registan Desert. Due to the region's complex topography and the nearby dust sources, air pollutants and airborne dust tend to accumulate, leading to significant environmental challenges (Chen et al., 2013b).

2.2. Polarization lidar system

The lidar system at Shaartuz Station was developed by Lanzhou University, China, as shown in Fig. 2. The system utilizes a Nd:YAG laser to emit laser pulses at wavelengths of 532 nm and 1064 nm, with a pulse repetition rate of 10 Hz. As the laser propagates through the atmosphere, it interacts with atmospheric constituents, resulting in backscattered echo signals that are collected by a Cassegrain reflector telescope with an aperture of 400 mm. The system captures both the perpendicular and parallel echo signals at 532 nm, as well as the total echo signal at 1064 nm, using photomultiplier tubes and an avalanche photodiode. Subsequently, the data are stored by the data acquisition module. The lidar system has a detection height range of 0–20 km, with a blind zone of approximately 120 m, a time resolution of 2 min, and a vertical resolution of 7.5 m. We applied the experimental method for overlap correction (Shimizu et al., 2004). Furthermore, the lidar data products include the attenuated backscattering coefficients at 1064 nm (β'_{1064}) and 532 nm (β'_{532}), depolarization ratio at 532 nm (δ_{532}), the color ratio (CR; $\beta'_{1064}/\beta'_{532}$), and the aerosol extinction coefficient at 532 nm (EXT_{532}). The calibration factor of δ_{532} can be determined by the atmospheric molecular method used in the authors' previous study (Dong et al., 2022; Liu et al., 2024; Zhang et al., 2023). EXT_{532} was derived by Fernald's method with a fixed lidar ratio of 50 sr (Fernald, 1984). We calculate the dust mass concentration (DMC) from the aerosol backscatter coefficient with dust mass extinction efficiency (0.45 m^2g^{-1}, in this study) according to the method described by Wang et al. (2021).

2.3. Surface observations

The CIMEL sun-sky-lunar photometer (CE318-T) is capable of providing aerosol quantification and physical-optical property parameters through automatic observations conducted both during the day and at night (Barreto et al., 2019; Perrone et al., 2022). This instrument is recognized for its high accuracy and is widely utilized in the fields of atmospheric science and environmental monitoring (Bi et al., 2025). The CE318-T features eight channels that encompass the visible light spectrum and extend into the near-infrared range. Its primary applications include the measurement of direct solar irradiance, nocturnal lunar irradiance, and aerosol optical depth (AOD). The Ångström exponent (AE) serves as an indicator of the wavelength dependence of AOD (Ångström, 1929), typically derived from AOD measurements within the spectral range of 440–870 nm (Barreto et al., 2016). The AE provides insights into the size of aerosol particles, with lower values indicating

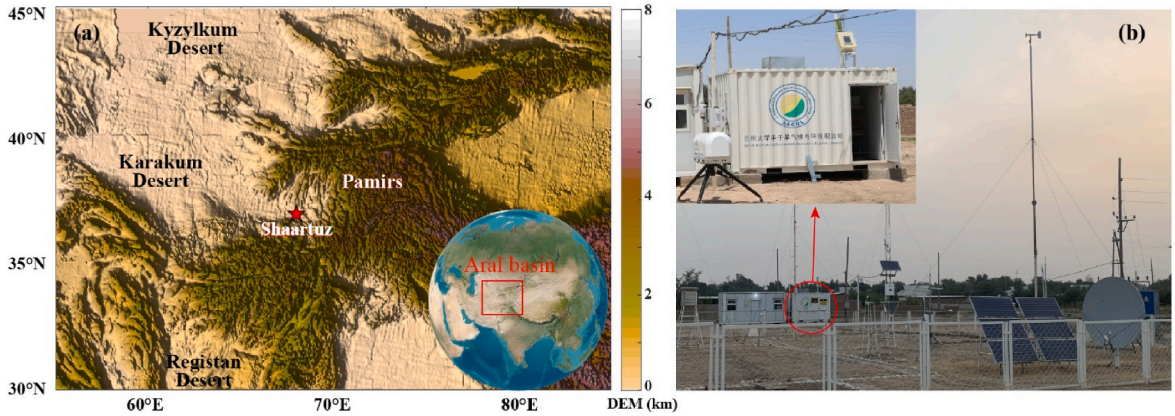

Fig. 1. (a) Geographic location (red five-pointed star) with topographical context and (b) photographs of Shaartuz Station which has been established for investigating distribution of dust aerosols and the sources.

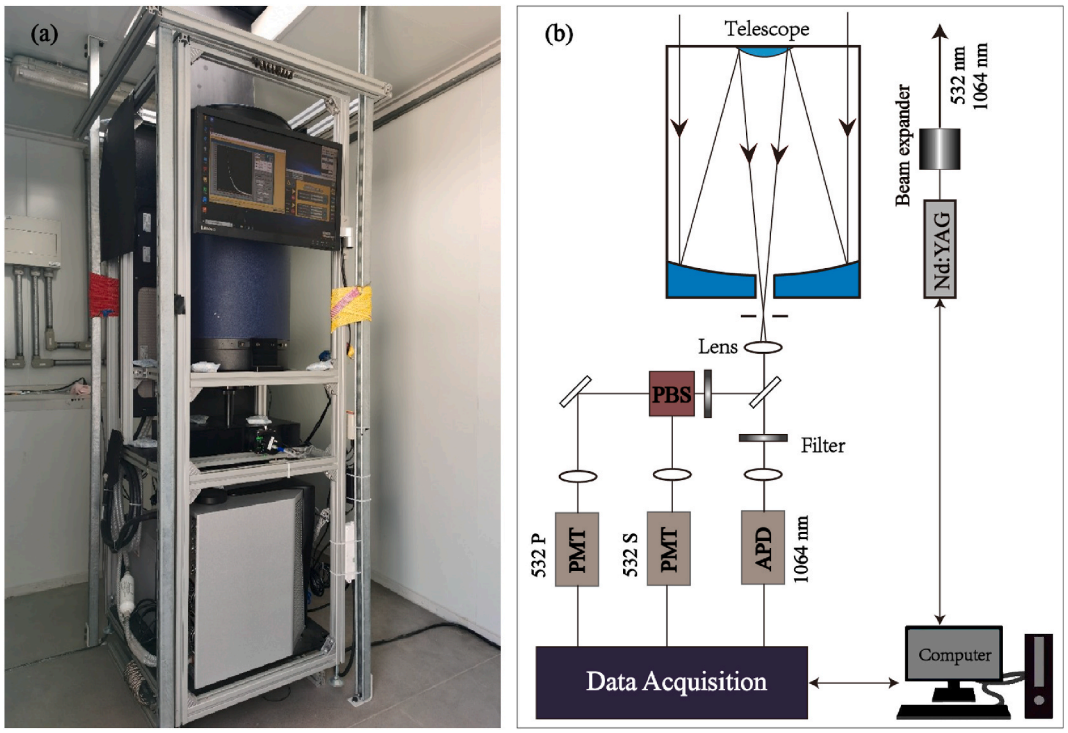

Fig. 2. (a) Photographs and (b) Schematic diagram of the ground-based polarization lidar system developed by Lanzhou University of China used in this study.

the presence of coarser particles. Furthermore, by employing the spectral deconvolution algorithm (SDA), AOD can be further partitioned into coarse and fine modes, thereby enhancing the understanding of the various aerosol components present in the atmosphere (Ma et al., 2024). In this study, AE is retrieved within the wavelength range of 440–870 nm, and the SDA is applied to ascertain the contributions of fine and coarse mode AOD at 500 nm, facilitating an analysis of the distribution of coarse and fine mode particles. No nighttime observations were available during the study period due to the lunar cycle. Additionally, to enhance the comparison of AOD observations, this study also includes 500 nm AOD data from the Dushanbe station, retrieved from the AERONET (Aerosol Robotic Network) database.

The Grimm EDM180 (Environmental Dust Monitor) is a professional air quality monitoring device produced by GRIMM AEROSOL TECHNIK Ainring GmbH & Co. KG, designed for the real-time measurement of airborne particulate matter concentrations. This device employs the principle of light scattering to determine particle size, providing size-resolved number concentrations across 31 channels, ranging from 0.25 μm to 32 μm. Utilizing the number concentration data, the mass concentrations of PM_{10}, $PM_{2.5}$, and PM_1 can be calculated through established modeling techniques. In comparison to other physical measurement methods, the Grimm EDM180 not only delivers a more rapid response time but also improves detection accuracy. In this study, observations from the Grimm EDM180, recorded at 5-min intervals, are employed to assess the concentrations of PM_{10} and $PM_{2.5}$ during a dust event.

The automatic meteorological observational device is employed in this context. It comprises various components, including infrared temperature sensors, barometers, humidity and temperature probes, and wind sensors. This device is capable of measuring several meteorological parameters, such as atmospheric pressure, temperature, humidity, wind speed, and wind direction. In this study, meteorological data with a temporal resolution of 30-min averages are utilized.

2.4. Auxiliary data

In this study, the Modern-Era Retrospective analysis for Research and Applications, Version 2 (MERRA-2) has been utilized, which represents the most recent reanalysis Earth system model developed by National Aeronautics and Space Administration (NASA, https://gmao.gsfc.nasa.gov/reanalysis/MERRA-2/). The MERRA-2 dataset spans from 1980 to the present and provides global coverage with a spatial resolution of 0.5° × 0.625° and a temporal resolution of 1 h (Gelaro et al., 2017). This dataset includes a variety of meteorological variables and aerosol products, such as temperature, humidity, wind speed, and radiation, and is extensively employed in climate research and weather forecasting (Buchard et al., 2017). In this study, AOD at 550 nm is utilized to examine the spatial distribution and seasonal variations of aerosols over the study area from 2020 to 2023.

Additionally, the HYSPLIT trajectory model is employed, which uses meteorological data from the Global Data Assimilation System (GDAS) as input (Stein et al., 2015). This model is frequently applied in atmospheric science research to trace aerosol sources and predict the dispersion and impact of pollutants (Huang et al., 2015; Liu et al., 2022). By analyzing the backward trajectories of air masses for 48 h originating from Shaartuz Station, the potential sources of dust aerosols are identified in southern Tajikistan. All data presented in this study are based on Coordinated Universal Time (UTC), which corresponds to local time in Tajikistan (LT = UTC+5), thereby facilitating analysis and ensuring consistency.

3. Results and discussion

3.1. Regional characteristics of AOD

Fig. 3 illustrates the seasonal evolution and monthly variation of AOD derived from the MERRA-2 reanalysis and AERONET data for the period spanning 2020 to 2023. The extensive arid desert regions of Central Asia contribute significantly to the influx of dust particles into the atmosphere throughout the year, resulting in elevated AOD levels. The annual average AOD at 550 nm recorded at the Shaartuz Station exceeds 0.3. In Fig. 3(a)–3(d), AOD at 550 nm exhibits pronounced seasonal variation trends across Central Asia, with peak values observed in spring and minimal values in winter. Notably, AOD values in the Amu Darya Basin during the summer months are comparable to those in spring, reaching the highest levels observed across all four seasons. This observation aligns with previous studies regarding the impact of dust in the region (Hofer et al., 2017). The monthly variation of AOD at the Shaartuz Station is determined by averaging the data from the three grid points nearest to the station. The Dushanbe Station, which is also located within the basin and in close proximity, provides additional context. In Fig. 3(e), AOD levels at the Shaartuz Station during the months of May to July are relatively high, while the Dushanbe Station similarly records its peak AOD for the year during this period. Although the AOD data utilized for both stations differ, the overall trend of monthly variation is effectively represented. Rupakheti et al. (2023) reported seasonal average AOD values over Dushanbe from 2010 to 2018, which similarly indicated that summer AOD levels are the highest, attributed to elevated temperatures, drought conditions, and increased wind activity during the summer months in the Central Asia region. Therefore, a representative dust event occurring in summer was selected for a comprehensive investigation of dust aerosol evolution in this study.

3.2. Time evolution of dust event

In this study, the initial dust outbreak recorded since the establishment of the Shaartuz Station (i.e., a persistent episode from July 19 to July 26, 2023) was selected for detailed analysis. During this period,

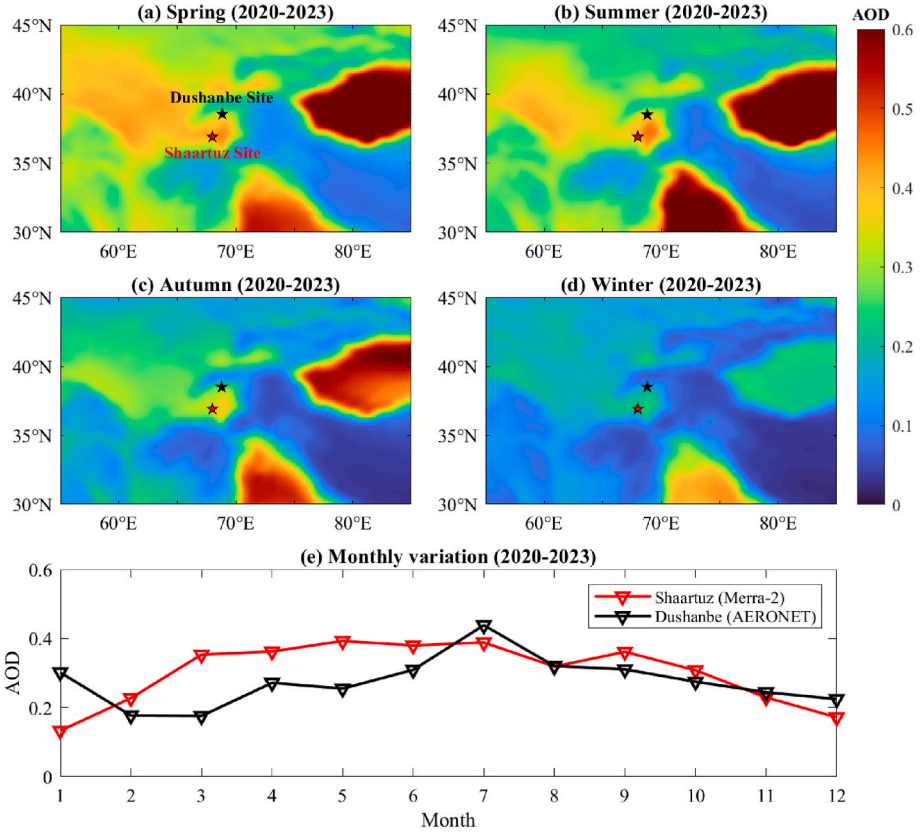

Fig. 3. (a–d) Seasonal average of AOD at 550 nm derived from MERRA-2 dataset during 2020–2023; (e) Monthly variation of AOD at Shaartuz (MERRA-2) and Dushanbe (AERONET) stations during 2020–2023.

MODIS observations also captured the dust event, with elevated AOD values (550 nm) reaching 1.1 on 19 July, indicating the presence of a strong dust storm (not shown here). In Fig. 4(a), concentrations of PM_{10} and $PM_{2.5}$ exhibited significant variability throughout the event, ranging from over 3000 μg/m^3 to below 100 μg/m^3. On July 19, PM_{10} ($PM_{2.5}$) mass concentrations rapidly increased, reaching two peaks of 3072.9 (477.6) μg/m^3 at 07:25 UTC (LT: 12:25) and 3841.7 (695.4) μg/m^3 at 13:10 UTC (LT: 18:10), respectively. The daily mean concentrations on that day were 1462.0 μg/m^3 for PM_{10} and 321.6 μg/m^3 for $PM_{2.5}$. Although the highest dust loadings occurred briefly, the event exerted a sustained impact on near-surface particle concentrations, as evidenced by the elevated daily averages observed on July 20, which reached 233.9 μg/m^3 for PM_{10} and 66.4 μg/m^3 for $PM_{2.5}$, with respective intraday peaks of 524.1 μg/m^3 and 107.9 μg/m^3. In the subsequent days, several minor peaks with concentrations below 500 μg/m^3 were recorded, exhibiting clear diurnal variation. However, the daily mean PM_{10} concentrations hovered approximately 100 μg/m^3, suggesting that these fluctuations were governed by mechanisms different from those responsible for the initial dust storm. However, the relatively elevated levels of PM_{10} and $PM_{2.5}$ during this period were closely linked to the residual effect of the July 19 event. The surrounding complex topography (i.e., characterized by high mountains on three sides) facilitated the accumulation of airborne dust once transported into the Amu Darya Basin, and further contributed to the persistence of high near-surface particle concentrations through boundary layer processes. This prolonged impact of the dust storm on atmospheric particle distribution is further supported by the particle number and mass concentration profiles in Fig. 4(b) and (c), where coarse particles (>10 μm) continued to be present throughout the observation period, albeit at lower concentrations, indicating a consistent contribution of coarse-mode dust. Therefore, based on the temporal variations in PM concentrations, particle number and mass size distributions, the dust event was classified into two phases: an intense dust phase from July 19 to 20, and a weaker dust phase spanning July 21 to 26.

In Fig. 5, wind speed showed a gradual decreasing trend, fluctuating between 0.3 m/s and 7.6 m/s. Concurrently, daily maximum temperatures consistently surpassed 40 °C, exhibiting a persistent upward trajectory, with values ranging from 40.7 °C to 48.6 °C throughout the study period. Notably, westerly winds prevailed, with wind speeds varying between 2.5 m/s and 7.6 m/s, demonstrating minimal diurnal variation during the intense dust stage occurring from July 19 to 20. These meteorological conditions facilitated the continuous transport and accumulation of dust particles from the adjacent desert into the basin. Impacted by elevated near-surface dust concentrations, nocturnal temperatures remained consistently above 30 °C from July 19 to 20, accompanied by a limited diurnal amplitude in both temperature and relative humidity. In contrast, during the weak dust stage from July 21 to 26, wind speeds predominantly remained below 4 m/s, characterized by rapid alternations between westerly and easterly winds. The amplitudes of diurnal fluctuations in wind speed, temperature, and relative humidity progressively intensified.

To conduct a comprehensive analysis of the columnar optical properties of aerosols at the Shaartuz Station during the dust event, continuous measurements were performed using the CE318 instrument. Fig. 6 depicts the temporal variations in aerosol spectral parameters. The spectral AOD values were predominantly distributed between 0.2 and 1.3. The AE values ranged from 0.2 to 0.5, with an overall average of 0.26 ± 0.07, while the fine-mode fraction (FMF) remained below 0.42. This observation indicates that coarse particles predominantly characterized the aerosol composition throughout the study period, which aligns with the typical characteristics of dusty environments. The low AE values (mean of 0.26) are indicative of mineral dust dominance, as an AE value of less than 0.5 is widely recognized as a robust indicator of coarse-mode aerosols (Dubovik et al., 2002; Eck et al., 2010). The overall mean value of AOD_{500} was 0.48 ± 0.18, which is higher than the annual and summer average levels recorded at many stations in Central Asia, and closely resembles the values observed during dust events in the region (Bi et al., 2016; Chen et al., 2013a; Ningombam et al., 2019). During the intense dust stage (July 19–20), the AOD across all wavelengths exceeded 0.5, with a mean AOD_{500} of 0.84 and a peak value of 1.25, which is comparable to the AOD_{500} of 1.3 observed at Shaartuz during dust storms by Fraser (1993).

This emphasizes the severity of the dust event, comparable to severe dust storms documented in arid regions (Hofer et al., 2017; Tao et al.,

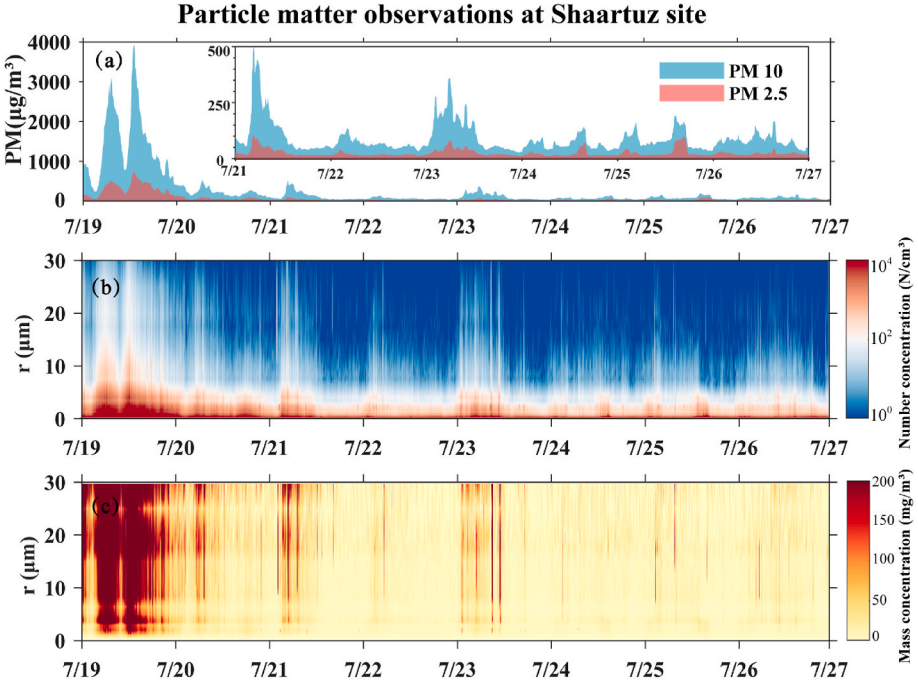

Fig. 4. Time series of particulate matter characteristics during the dust event from July 19 to 26, 2023: (a) Mass concentration of PM_{10} and $PM_{2.5}$; (b) Particle number size distributions; (c) Particle mass size distributions detected by the ground-based Grimm EDM 180 at Shaartuz site.

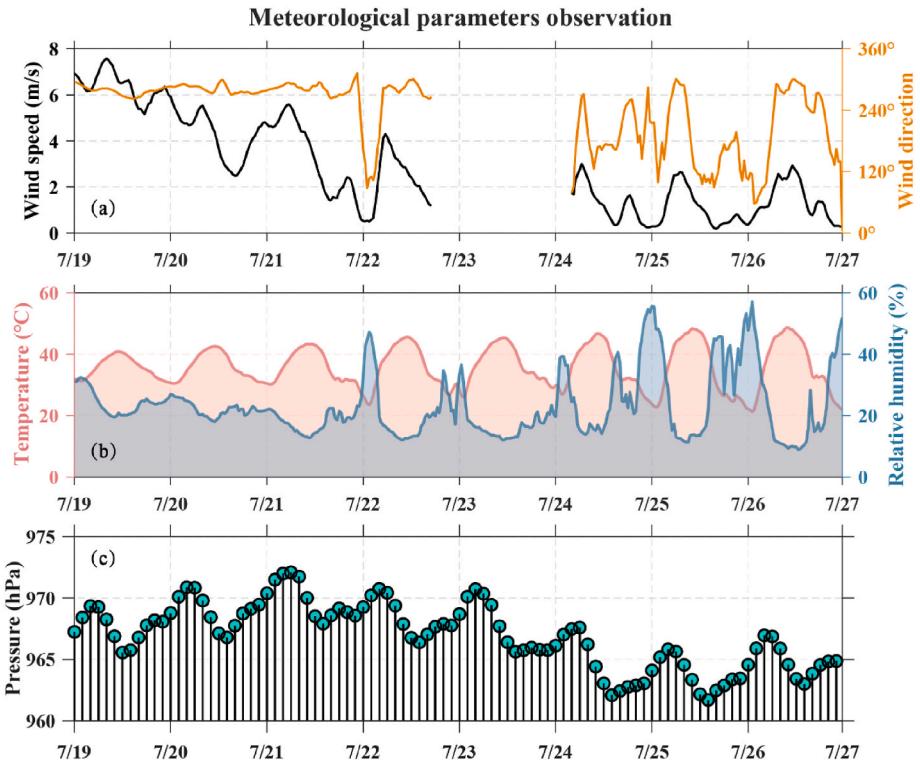

Fig. 5. Temporal evolutions of near-surface meteorological conditions measured by the automatic meteorological observational device during the dust event from July 19 to 26: (a) Wind speed (black) and wind direction (orange); (b) Air temperature (red) and relative humidity (blue); (c) Atmospheric pressure.

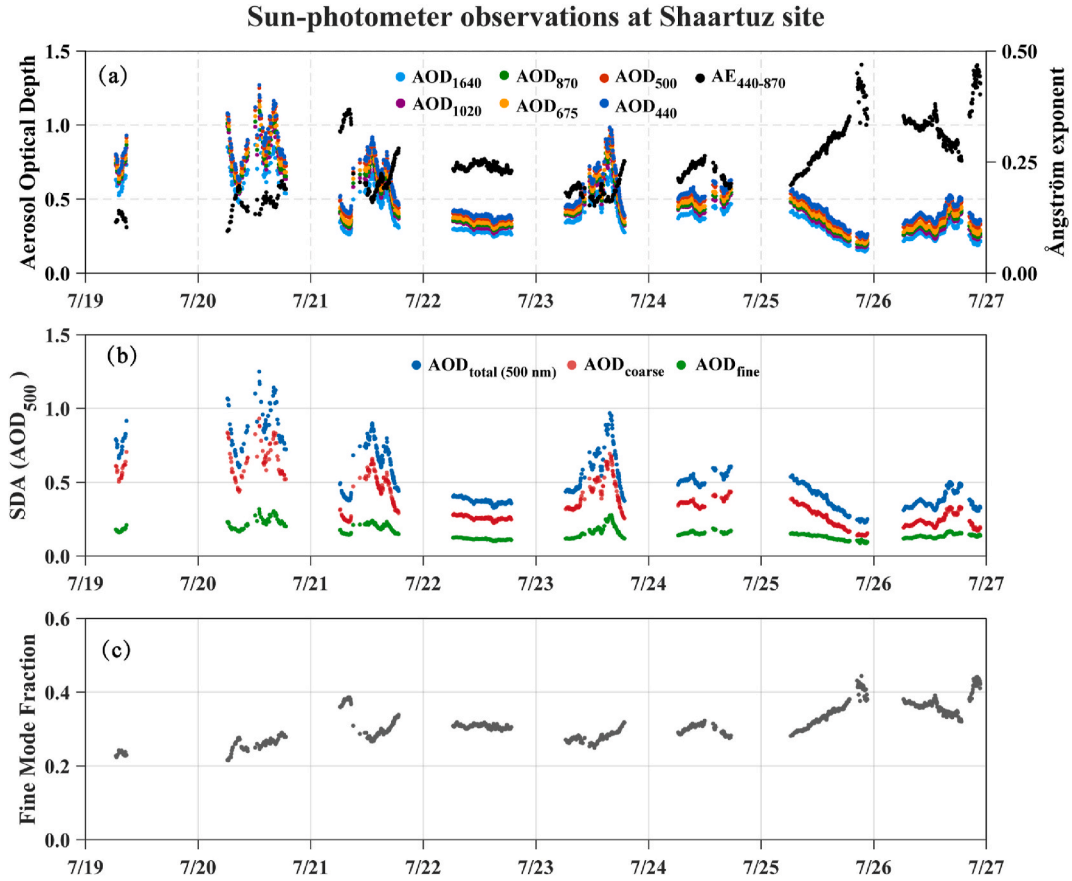

Fig. 6. Time series of columnar aerosol optical properties at Shaartuz Station from July 19 to 26, 2023: (a) Spectral AOD at multiple wavelengths and Ångström exponent (440–870 nm); (b) Coarse-mode (red), fine-mode (green), and total (blue) AOD at 500 nm based on SDA; (c) FMF based SDA.

2022; Wang et al., 2023). The AE during this period was below 0.2, remaining exceptionally low with an average of 0.16 (0.09–0.21), while the FMF consistently fell below 0.3. Notably, the AE values approached those reported for pure dust events (Schuster et al., 2006; Zhou et al., 2018; Zhu et al., 2017), suggesting minimal impact from fine-mode pollutants during the intense dust process. In contrast, during the weak dust stage, AOD exhibited a reduction across all wavelengths compared to the severe dust phase. Concurrently, the AE increased significantly, particularly on July 25–26, with a mean of 0.30 and a maximum of 0.47. This inverse relationship between AOD and AE magnitudes reveals fundamental shifts in aerosol composition, characterized by decreasing coarse dust loadings accompanied by increasing contributions from fine-mode particles.

The high spatio-temporal resolution of lidar technology has facilitated the investigation of the vertical distribution of aerosols in southern Tajikistan during dust events. Fig. 7 illustrates the diversity and complexity of dust layers observed above the Shaartuz Station through ground-based polarization lidar measurements. It includes the attenuated backscattering coefficients at wavelengths of 1064 nm (β'_{1064}) and 532 nm (β'_{532}), linear volume depolarization ratio at 532 nm (δ_{532}), and CR ($\beta'_{1064}/\beta'_{532}$). The attenuated backscattering coefficient serves as an indicator of the distribution of aerosol concentrations, while the presence of dust aerosols can be identified through lidar profiles of δ_{532}. The higher δ_{532} values suggest an increased degree of non-sphericity and irregularity of particle shapes. CR can be employed to characterize particle size, with larger CRs correlating with larger particle sizes (Dong et al., 2022; Zhang et al., 2022).

On July 19, significant aerosol backscattering was recorded at heights below 1 km near the surface, with δ_{532} exceeding 0.4 and CR values greater than 1.5. These values of δ_{532} are comparable to those observed in previous studies concerning dust particles over Asia (Chen et al., 2013b; Heese et al., 2022; Hofer et al., 2017; Zhou et al., 2021). This suggests that the near-surface aerosol particles exhibit significant irregular shape and that the overall particle size is relatively large, which aligns with the results in Fig. 4. While sun photometers and Grimm instruments are capable of measuring concentration and optical parameters in both the near-surface and atmospheric column, lidar observations indicate that a substantial amount of surface dust can be lifted into the atmosphere, with a non-uniform vertical distribution. Following the severe dust storm on July 20, the dust plume was characterized by relatively low aerosol loadings at the surface and different stratification of dust layers. Lidar technology enables the monitoring of the diffusion and transport processes of dust in the vertical dimension. The presence of multiple layers of dust aerosols can be identified through the analysis

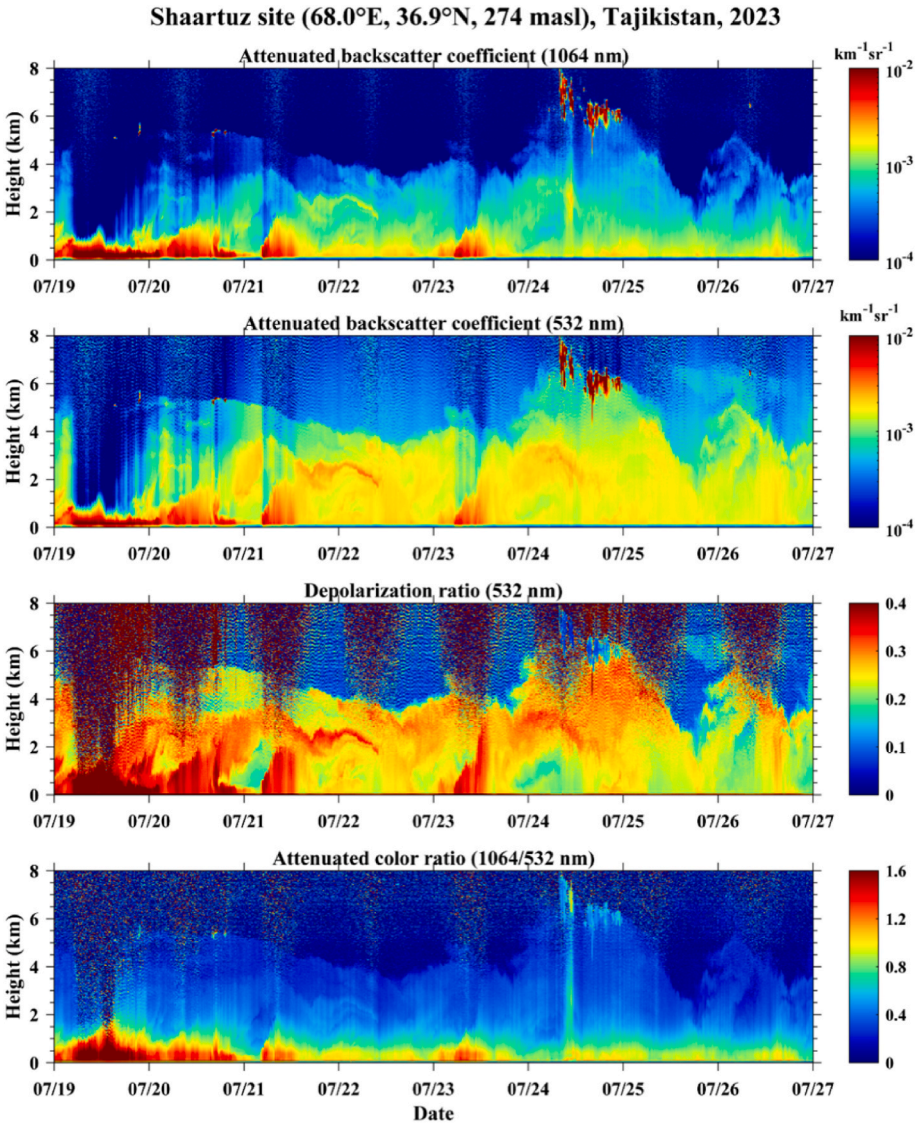

Fig. 7. Time-height cross section of the dust event observed by ground-based polarization lidar at Shaartuz Station from July 19 to 26, 2023.

of δ_{532} and CR values. Dust aerosols near the ground were observed to rise and extend upward to approximately 5 km. The attenuated backscattering coefficients suggest the existence of moderately thick aerosol layers below approximately 2 km. At around 4:00 on July 23, aerosol loadings near the surface increased once again, with most particles exhibiting significant irregular shape and larger sizes. Between July 24 and 25, conditions for pollution dispersion improved, as a higher atmospheric boundary layer facilitated the vertical diffusion of dust. The dust aerosols were elevated to approximately 5.5 km above ground level, and the elevated particles showed relatively high depolarization ratios ($\delta_{532} > 0.25$). Since 12:00 on July 25, the loading of dust aerosols gradually decreased at both high heights and near the ground.

To perform a quantitative analysis of the aerosol optical properties and the vertical distribution of DMC during the dust event, average profiles for the aerosol extinction coefficient at 532 nm (EXT_{532}), δ_{532}, CR, and DMC for two time periods are illustrated in Fig. 8: (1) the intense dust stage (red line, from 12:00 to 18:00 on July 19); and (2) the weak dust stage (blue line, from 0:00 to 4:00 on July 25). During the dust event that commenced on July 19, aerosol concentrations near the surface exhibited a significant increase. The EXT_{532} exceeded 0.5 km^{-1} and subsequently decreased with height, indicating a high aerosol loading in the near-surface layer. Dust particles concentrated below 1 km during this period were predominantly coarse-mode aerosols, likely resulting from short-range transport from nearby desert sources. On July 25, the intensity of the dust event diminished considerably, leading to a reduction in aerosol concentrations. In comparison to the intense dust stage, the EXT_{532} below 4.2 km remained relatively stable at approximately 0.4 km^{-1}. Analysis of the average profiles of δ_{532} and CR revealed that irregularity and particle size continued to decrease with height on July 19. The non-sphericity of aerosol particles below 3 km was higher ($\delta_{532} > 0.25$), while the particle size of aerosols below 1.5 km was larger (CR > 0.5). On July 25, as aerosols were distributed at higher heights, the maximum δ_{532} was observed at 4.2 km, approximately 0.3. Such high depolarization ratios indicate almost pure dust conditions, characterized by non-spherical particles with high reflective properties. In Fig. 8(d), the maximum DMC near the surface reached 1500 $\mu g/m^3$ during the dust event. DMC remained relatively stable between approximately 1.5 and 3 km on 19 July, suggesting a sustained presence of dust within the upper layer. The mass loading of dust was greatest at an height of 4.2 km on July 25, the concentration reached 800 $\mu g/m^3$.

Fig. 9 depicts the frequency distribution of the δ_{532} and CR values during the observation period (19–26 July 2023). The results indicate that the δ_{532} predominantly range from 0.2 to 0.35, with a mean value of 0.27 ± 0.05. In contrast, the CR values range from 0.25 to 0.75, with an average value of 0.50 ± 0.49. These results are consistent with the typical depolarization ratios associated with dust, suggesting that dust aerosols were the predominant type during the observation period (Haarig et al., 2022; Kim et al., 2010; Yin et al., 2021). In Fig. 9(c) and (d), there are more particles with δ_{532} exceeding 0.35 below 2 km compared to those above 2 km. However, the overall trend indicates that δ_{532} increase with height. At heights below 2 km, the lower δ_{532} are predominantly distributed within the range of 0.2–0.28. Conversely, at heights between 2 and 4 km, these values are found within the range of 0.25–0.32. This observation suggests that a substantial number of dust particles have been elevated to heights exceeding 2 km during the dust event. CR values exhibit a significant change with height, demonstrating a gradual decrease as height increases. This trend indicates that larger aerosol particle sizes are more prevalent near the surface. A significant change in CRs is observed at approximately 2 km. Below this height, CR values decrease more rapidly with increasing height, whereas between 2 km and 4 km, the change is more gradual.

3.3. Statistical characteristics of dust event

Based on the distribution in Fig. 9, significant differences are observed in the δ_{532} and CR of aerosols at heights above and below approximately 2 km. In this study, the HYSPLIT model is employed to simulate the backward trajectory of airflow over a 48-h period for two specific height ranges: 0.4–1.6 km and 2.2–4 km. The vertical interval for the trajectories is set at 200 m, while the temporal interval is 1 h. By analyzing the frequency of these trajectories at identical locations, the primary transport pathways and potential sources contributing to dust can be identified (Fig. 10). The trajectories reveal that within the height range of 0.4–1.6 km, there are two predominant airflow pathways: the

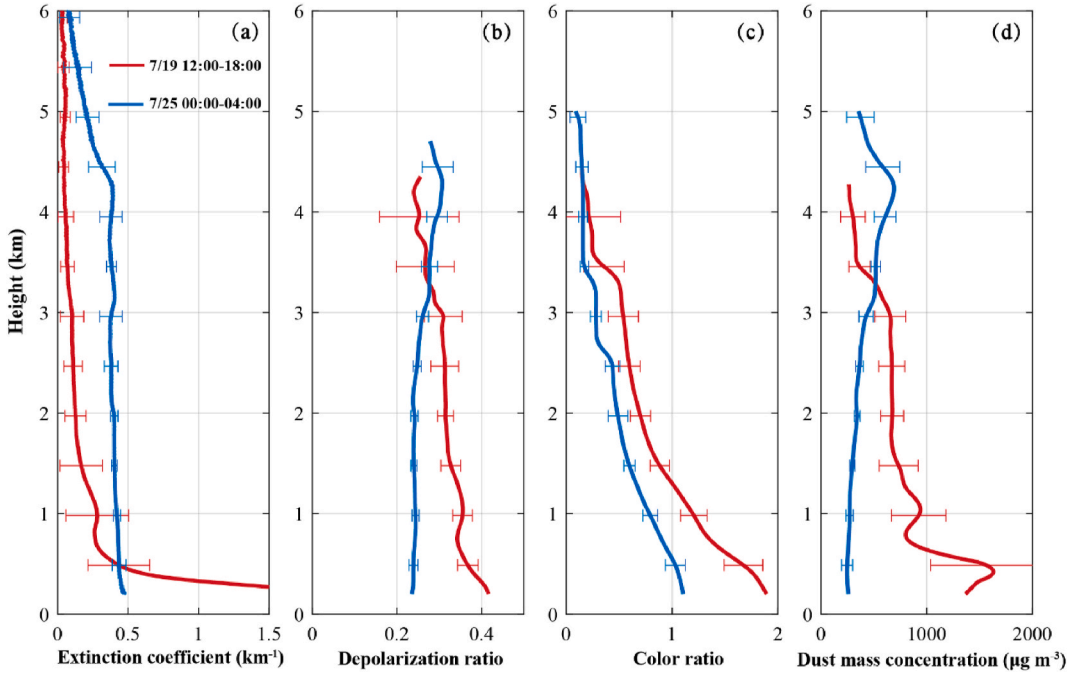

Fig. 8. Mean vertical profiles of aerosol properties during two phases of the dust event: (a) Aerosol extinction coefficient at 532 nm; (b) Depolarization ratio; (c) Color ratio; (d) Dust mass concentration. (Note: Red lines represent the intense dust stage (12:00–18:00 on July 19), and blue lines represent the weak dust stage (00:00–04:00 on July 25)).

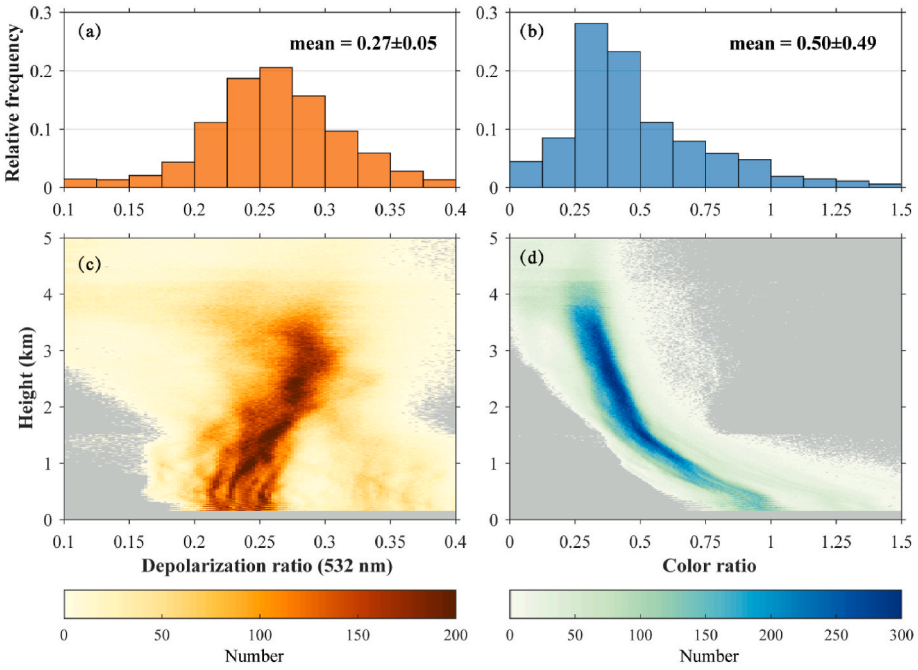

Fig. 9. Histogram distribution and density scatterplots for depolarization ratio and color ratio measured by ground-based polarization lidar from July 19 to 26, 2023.

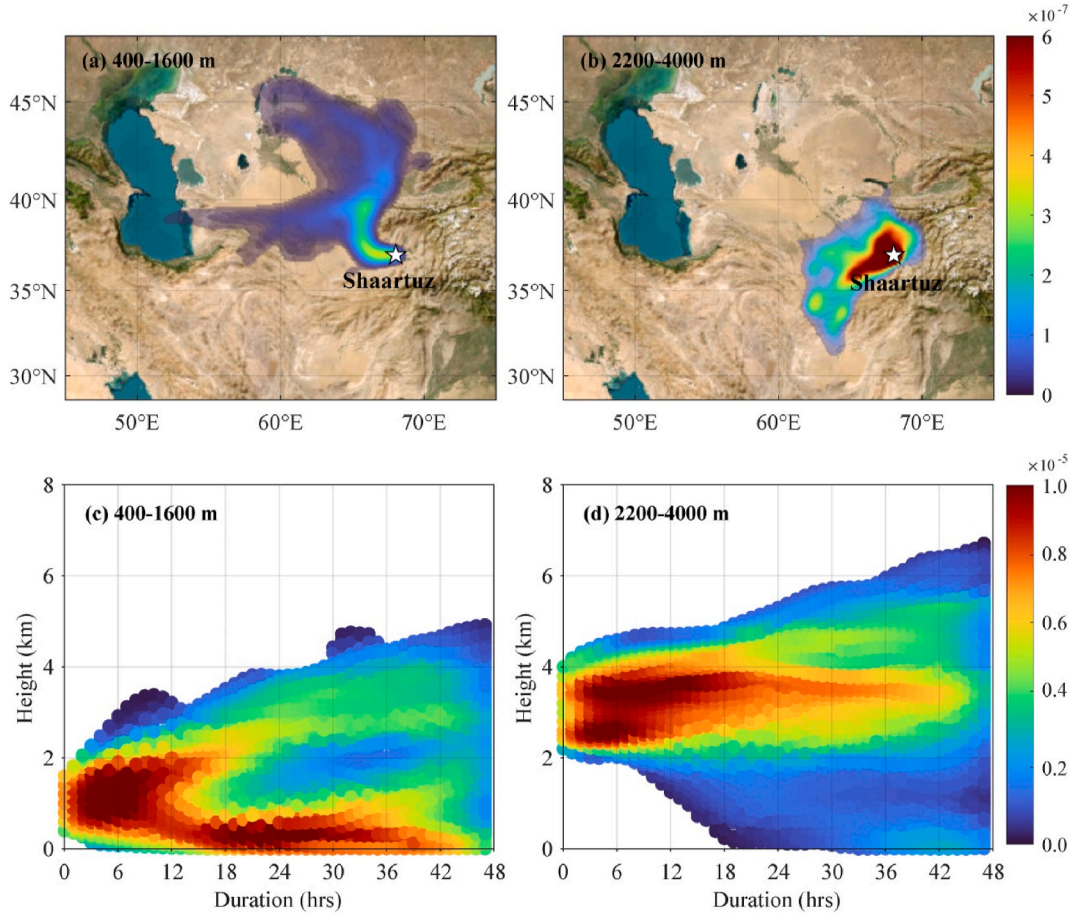

Fig. 10. (a,b) Probability density distribution of 48-h backward trajectories of dust layer airflows at 0.4–1.6 km and 2.2–4.0 km; (c,d) Height density distributions of airflow trajectories arriving at Shaartuz Station from July 19 to 26, 2023.

northern pathway and the western pathway (Fig. 10(a)). These airflows converge at the entrance to the Amu Darya Basin before proceeding eastward toward the monitoring station. The airflow along the northern pathway traverses the Kysylkum Desert in Uzbekistan, whereas the airflow along the western pathway passes through the Karakum Desert. These desert regions are significant contributors to the dust aerosols transported to southern Tajikistan within the 48-h timeframe. In Fig. 10 (c), the backward trajectory airflow is predominantly distributed below 4 km, with a majority of the airflow continuously ascending from the ground level. The airflow within the 2.2–4 km range follows the southern pathway, originating from the arid desert regions of Afghanistan. Due to the impact of topography, the distribution of airflow along the southern pathway is relatively elevated, mainly concentrated between 2 and 6 km (Fig. 10(d)). Considering Tajikistan shares a southern border with Afghanistan, it is plausible that dust aerosols originating from the arid regions of Afghanistan may be transported by wind to the Shaartuz Station, particularly during seasons characterized by high wind speeds or frequent sandstorms (Rupakheti et al., 2020b).

Fig. 11 illustrates the relationship between parameters EXT_{532}, δ_{532} and CR across different height ranges (0.4–1.6 km and 2.2–4 km), as well as the corresponding probability density distributions. It can be concluded that there are significant differences in aerosol particle characteristics across various height ranges. The overall distribution of aerosol particles at lower heights δ_{532} ranges from 0.2 to 0.4, with a peak probability density of approximately 0.27. The CRs for these particles are consistently greater than 0.5, reaching a maximum 0.74. In contrast, EXT_{532} exhibit a more concentrated distribution, specifically between 0.3 km^{-1} and 0.5 km^{-1}, with a maximum value of 0.41 km^{-1}. The results suggest that near-surface aerosol particles are generally larger in size, exhibiting higher depolarization ratio and increased aerosol loading, as well as enhanced light attenuation. Specifically, in Fig. 11(b), aerosol particles at heights ranging from 2.2 km to 4 km are characterized by smaller particle sizes, with a CR of less than 1, predominantly concentrated between 0.4 and 0.6, and a peak probability density of approximately 0.55. Compared with Fig. 11(a), δ_{532} in Fig. 11(c) has a wider distribution range and a significant increase in the number of particles exhibiting a depolarization ratio of less than 0.2, reaching a maximum value of 0.28. Furthermore, in Fig. 11(d), the probability density peak of the extinction coefficient within the 2.2–4.0 km range is observed at 0.37 km^{-1}, accompanied by two smaller peaks at 0.15 km^{-1} and 0.5 km^{-1}. Additionally, EXT_{532} demonstrates positive correlations with δ_{532} and CR. The results suggest that the EXT_{532} increases not only with the non-sphericity of particles but also with particle size, which aligns with the observations made by Hofer et al. (2020) in Dushanbe.

4. Conclusions

This study presents a comprehensive investigation into the

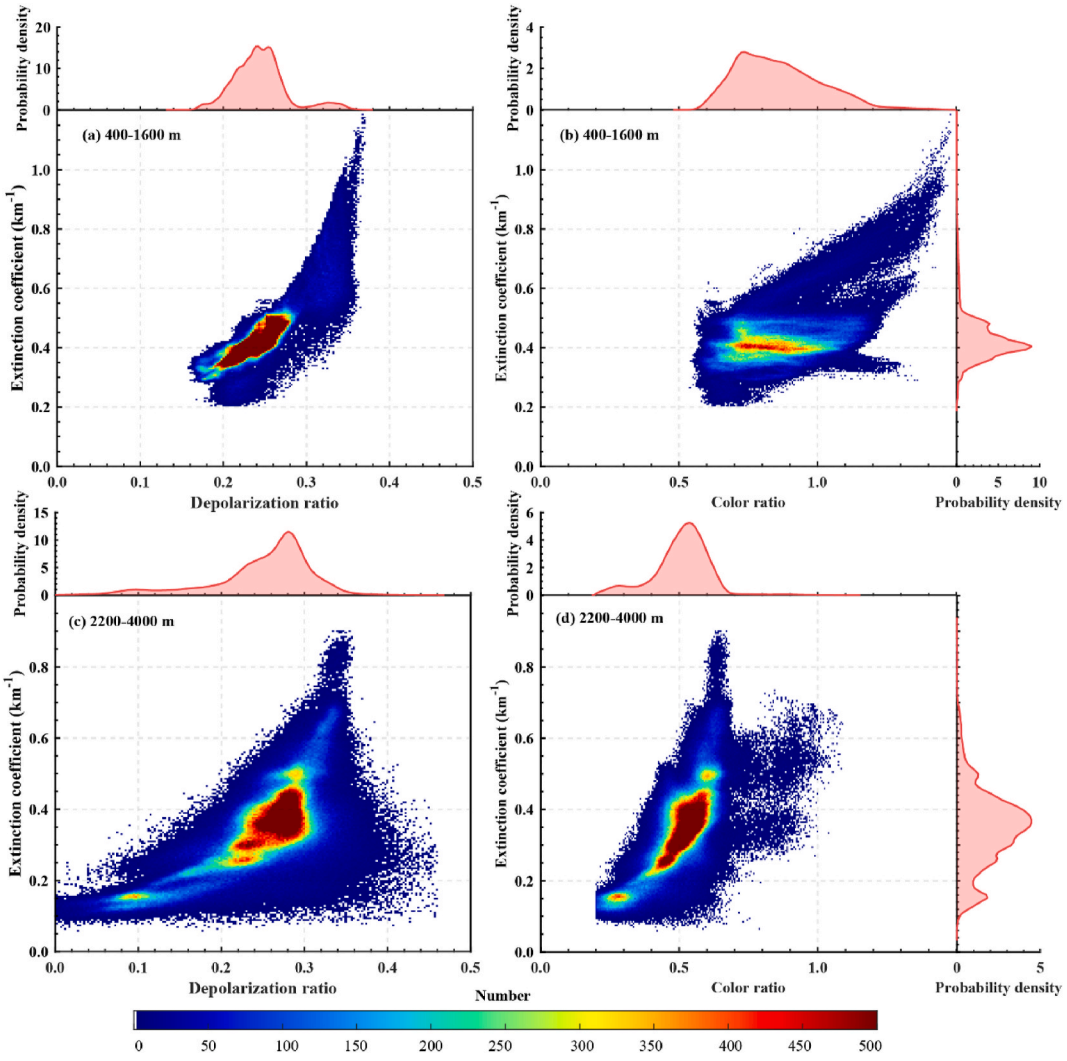

Fig. 11. Correlation between aerosol extinction coefficient at 532 nm and (a,c) depolarization ratio and (b,d) color ratio at different height ranges, along with corresponding probability density distributions based on observations from 19 to July 26, 2023.

spatiotemporal distribution and optical characteristics of dust aerosols during a prolonged dust episode observed from July 19 to 26, 2023, at the Shaartuz Station in southern Tajikistan. The results reveal a sustained presence of coarse-mode particles, with number and mass concentrations for particles sizes exceeding 10 μm remaining significant throughout the observational period. The event was divided into two stages: an intense dust stage (July 19–20) and a weaker dust stage (July 21–26). The dust storm outbreak on July 19 led to peak PM_{10} and $PM_{2.5}$ concentrations of 3841 $\mu g/m^3$ and 695 $\mu g/m^3$, respectively. Westerly winds during the intense stage facilitated continuous dust transport from nearby deserts into the Amu Darya Basin, with dust accumulation occurring below 1 km and dominated by coarse-mode aerosols. During the weaker stage, dust loading decreased, while fine-mode contributions increased, accompanied by a clear vertical stratification of the dust plume extending up to 5 km.

Statistical analyses of the depolarization ratio and CR from lidar measurements revealed a two-layer vertical dust structure during the dust event. The lower layer (0.4–1.6 km) was impacted by northerly and westerly airflows transporting dust from the Kyzylkum and Karakum Deserts, while the upper layer (2–4 km) was sustained by southerly airflows from arid regions of Afghanistan. Near-surface aerosols were characterized by larger and more irregularly shapedparticles (depolarization ratio >0.2), indicating dominant mineral dust. The elevated layer exhibited a wider range of particle shapes, including a substantial fraction with depolarization ratios below 0.2, suggesting a significant influence of polluted dust.

Overall, this study offers important insights into the vertical distribution, transport pathways, and optical properties of dust aerosols in southern Tajikistan, contributing to the broader understanding of dust dynamics in Central Asia. However, the reliance on a single observation station imposes limitations on the spatial generalizability of the results. It should be noted that the two-layer structure identified in this study was observed during a single dust event. To confirm its representativeness and better quantify the contributions of different dust sources to total columnar concentrations, longer-term and multi-site observations are needed. Future research should integrate multi-station ground-based observations and satellite remote sensing to further characterize regional dust transport processes and their environmental and climatic implications.

CRediT authorship contribution statement

Zhongwei Huang: Writing – review & editing, Writing – original draft, Validation, Methodology, Investigation, Funding acquisition, Data curation, Conceptualization. **Qingqing Dong:** Writing – original draft, Visualization, Validation, Methodology, Investigation, Data curation. **Tian Zhou:** Writing – review & editing, Methodology, Funding acquisition, Data curation, Conceptualization. **Jianrong Bi:** Writing – review & editing, Methodology, Funding acquisition, Data curation. **Rui Chen:** Data curation. **Qiantao Liu:** Visualization, Data curation. **Sabur F. Abdullaev:** Data curation. **Dilovar Nozirov:** Data curation. **Khan Alam:** Writing – review & editing, Data curation. **Tianhe Wang:** Methodology, Conceptualization. **Wuren Li:** Conceptualization. **Ze Li:** Data curation. **Xiaodong Song:** Data curation. **Wentao Liu:** Data curation.

Data availability statement

All reanalysis data sets used in this research are openly available. The MERRA-2 data are available from the NASA Goddard Earth Sciences (GES) Data and Information Services Center (DISC) website (https://disc.gsfc.nasa.gov/). You need to register before downloading data. The AErosol RObotic NETwork (AERONET) provides globally distributed observations of spectral aerosol optical depth (AOD), which can be obtained from the AERONET website (https://aeronet.gsfc.nasa.gov/new_web/data.html). The installation of HYSPLIT trajectory model PC version is downloaded from NOAA Air Resources Laboratory website (https://www.ready.noaa.gov/documents/Tutorial/html/index.html). Other ground-based data can be accessed from the authors upon reasonable request.

Declaration of competing interest

The authors declare that they have no known competing financial interests or personal relationships that could have appeared to influence the work reported in this paper.

Acknowledgments

This work was jointly supported by the National Natural Science Foundation of China (W2411029 and 42475078), the Gansu Science and Technology Major Program (24ZDWA006), the Self-supporting Program of Guangzhou Laboratory (GZNL2024A01004), the '111 Center' (B25040) and Fundamental Research Funds for the Central Universities (lzujbky-2025-jdzx04). The authors gratefully acknowledge the NOAA Air Resources Laboratory for the provision of the HYSPLIT model, and NASA for providing MERRA data.

Data availability

Data will be made available on request.

References

Ångström, A., 1929. On the atmospheric transmission of sun radiation and on dust in the air. Geogr. Ann. 11, 156–166. https://doi.org/10.1080/20014422.1929.11880498.

Barreto, Á., Cuevas, E., Granados-Muñoz, M.-J., Alados-Arboledas, L., Romero, P.M., Gröbner, J., Kouremeti, N., Almansa, A.F., Stone, T., Toledano, C., Román, R., Sorokin, M., Holben, B., Canini, M., Yela, M., 2016. The new sun-sky-lunar cimel CE318-T multiband photometer – a comprehensive performance evaluation. Atmos. Meas. Tech. 9, 631–654. https://doi.org/10.5194/amt-9-631-2016.

Barreto, A., Román, R., Cuevas, E., Pérez-Ramírez, D., Berjón, A.J., Kouremeti, N., Kazadzis, S., Gröbner, J., Mazzola, M., Toledano, C., Benavent-Oltra, J.A., Doppler, L., Juryšek, J., Almansa, A.F., Victori, S., Maupin, F., Guirado-Fuentes, C., González, R., Vitale, V., Goloub, P., Blarel, L., Alados-Arboledas, L., Woolliams, E., Taylor, S., Antuña, J.C., Yela, M., 2019. Evaluation of night-time aerosols measurements and lunar irradiance models in the frame of the first multi-instrument nocturnal intercomparison campaign. Atmos. Environ. 202, 190–211. https://doi.org/10.1016/j.atmosenv.2019.01.006.

Bi, J., Huang, J., Holben, B., Zhang, G., 2016. Comparison of key absorption and optical properties between pure and transported anthropogenic dust over East and Central Asia. Atmos. Chem. Phys. 16, 15501–15516. https://doi.org/10.5194/acp-16-15501-2016.

Bi, J., Wang, X., Huang, Z., Abdullaev, S.F., Li, B., Meng, Z., Nozirov, D., Huang, J., 2025. Diurnal and nocturnal dust aerosol characteristics at ayvaj of southwest Tajikistan determined from Sun-Sky-Lunar photometric measurements. J. Geophys. Res. Atmos. 130, e2024JD042984. https://doi.org/10.1029/2024JD042984.

Bohlmann, S., Baars, H., Radenz, M., Engelmann, R., Macke, A., 2023. Ship-borne aerosol profiling with lidar over the Atlantic Ocean: from pure marine conditions to complex dust–smoke mixtures. Atmos. Chem. Phys. 18, 9661–9679. https://doi.org/10.5194/acp-18-9661-2018.

Buchard, V., Randles, C.A., da Silva, A.M., Darmenov, A., Colarco, P.R., Govindaraju, R., Ferrare, R., Hair, J., Beyersdorf, A.J., Ziemba, L.D., Yu, H., 2017. The MERRA-2 aerosol reanalysis, 1980 onward. Part II: evaluation and case studies. J. Clim. 30, 6851–6872. https://doi.org/10.1175/JCLI-D-16-0613.1.

Chen, B.B., Sverdlik, L.G., Imashev, S.A., Solomon, P.A., Lantz, J., Schauer, J.J., Shafer, M.M., Artamonova, M.S., Carmichael, G., 2013a. Empirical relationship between particulate matter and aerosol optical depth over northern tien-Shan, central Asia. Air Qual. Atmos. Health 6, 385–396. https://doi.org/10.1007/s11869-012-0192-5.

Chen, B.B., Sverdlik, L.G., Imashev, S.A., Solomon, P.A., Lantz, J., Schauer, J.J., Shafer, M.M., Artamonova, M.S., Carmichael, G.R., 2013b. Lidar measurements of the vertical distribution of aerosol optical and physical properties over central Asia. Int. J. Atmos. Sci. 2013, 1–17. https://doi.org/10.1155/2013/261546.

Chen, Feng, Chen, Y., Bakhtiyorov, Z., Zhang, H., Man, W., Chen, Fahu, 2020. Central Asian river streamflows have not continued to increase during the recent warming hiatus. Atmos. Res. 246, 105124. https://doi.org/10.1016/j.atmosres.2020.105124.

Chen, P., Kang, S., Zhang, L., Abdullaev, S.F., Wan, X., Zheng, H., Maslov, V.A., Abdyzhapar uulu, S., Safarov, M.S., Tripathee, L., Li, C., 2022. Organic aerosol compositions and source estimation by molecular tracers in Dushanbe, Tajikistan. Environ. Pollut. 302, 119055. https://doi.org/10.1016/j.envpol.2022.119055.

Chen, Y., Chen, S., Zhou, J., Zhao, D., Bi, H., Zhang, Y., Alam, K., Yu, H., Yang, Y., Chen, J., 2023. A super dust storm enhanced by radiative feedback. npj Clim. Atmos. Sci. 6, 1–11. https://doi.org/10.1038/s41612-023-00418-y.

Dong, Q., Huang, Z., Li, W., Li, Z., Song, X., Liu, W., Wang, T., Bi, J., Shi, J., 2022. Polarization lidar measurements of dust optical properties at the junction of the Taklimakan Desert–tibetan Plateau. Remote Sens. 14, 558. https://doi.org/10.3390/rs14030558.

Dubovik, O., Holben, B., Eck, T.F., Smirnov, A., Kaufman, Y.J., King, M.D., Tanré, D., Slutsker, I., 2002. Variability of absorption and optical properties of key aerosol types observed in worldwide locations. J. Atmos. Sci. 59, 590–608. https://doi.org/10.1175/1520-0469.

Eck, T.F., Holben, B.N., Sinyuk, A., Pinker, R.T., Goloub, P., Chen, H., Chatenet, B., Li, Z., Singh, R.P., Tripathi, S.N., Reid, J.S., Giles, D.M., Dubovik, O., O'Neill, N.T., Smirnov, A., Wang, P., Xia, X., 2010. Climatological aspects of the optical properties of fine/coarse mode aerosol mixtures. J. Geophys. Res. 115. https://doi.org/10.1029/2010JD014002.

Fernald, F.G., 1984. Analysis of atmospheric lidar observations: some comments. Appl. Opt. 23, 652. https://doi.org/10.1364/AO.23.000652.

Fraser, R.S., 1993. Optical thickness of atmospheric dust over Tadzhikistan. Atmos. Environ. 27, 2533–2538. https://doi.org/10.1016/0960-1686(93)90026-U.

Gelaro, R., McCarty, W., Suárez, M.J., Todling, R., Molod, A., Takacs, L., Randles, C.A., Darmenov, A., Bosilovich, M.G., Reichle, R., Wargan, K., Coy, L., Cullather, R., Draper, C., Akella, S., Buchard, V., Conaty, A., da Silva, A.M., Gu, W., Kim, G.-K., Koster, R., Lucchesi, R., Merkova, D., Nielsen, J.E., Partyka, G., Pawson, S., Putman, W., Rienecker, M., Schubert, S.D., Sienkiewicz, M., Zhao, B., 2017. The modern-era retrospective analysis for research and applications, version 2 (MERRA-2). J. Clim. 30, 5419–5454. https://doi.org/10.1175/JCLI-D-16-0758.1.

Haarig, M., Ansmann, A., Engelmann, R., Baars, H., Toledano, C., Torres, B., Althausen, D., Radenz, M., Wandinger, U., 2022. First triple-wavelength lidar observations of depolarization and extinction-to-backscatter ratios of Saharan dust. Atmos. Chem. Phys. 22, 355–369. https://doi.org/10.5194/acp-22-355-2022.

Heese, B., Floutsi, A.A., Baars, H., Althausen, D., Hofer, J., Herzog, A., Mewes, S., Radenz, M., Schechner, Y.Y., 2022. The vertical aerosol type distribution above Israel – 2 years of lidar observations at the coastal city of Haifa. Atmos. Chem. Phys. 22, 1633–1648. https://doi.org/10.5194/acp-22-1633-2022.

Hofer, J., Althausen, D., Abdullaev, S.F., Makhmudov, A.N., Nazarov, B.I., Schettler, G., Engelmann, R., Baars, H., Fomba, K.W., Müller, K., Heinold, B., Kandler, K., Ansmann, A., 2017. Long-term profiling of mineral dust and pollution aerosol with multiwavelength polarization Raman lidar at the Central Asian site of Dushanbe, Tajikistan: case studies. Atmos. Chem. Phys. 17, 14559–14577. https://doi.org/10.5194/acp-17-14559-2017.

Hofer, J., Ansmann, A., Althausen, D., Engelmann, R., Baars, H., Fomba, K.W., Wandinger, U., Abdullaev, S.F., Makhmudov, A.N., 2020. Optical properties of Central Asian aerosol relevant for spaceborne lidar applications and aerosol typing at 355 and 532 nm. Atmos. Chem. Phys. 20, 9265–9280. https://doi.org/10.5194/acp-20-9265-2020.

Huang, Z., Dong, Q., Chen, B., Wang, T., Bi, J., Zhou, T., Alam, K., Shi, J., Zhang, S., 2023a. Method for retrieving range-resolved aerosol microphysical properties from polarization lidar measurements. Opt. Express 31, 7599. https://doi.org/10.1364/OE.481252.

Huang, Z., Huang, J., Hayasaka, T., Wang, S., Zhou, T., Jin, H., 2015. Short-cut transport path for Asian dust directly to the Arctic: a case study. Environ. Res. Lett. 10 https://doi.org/20200031315141626.

Huang, Z., Li, M., Bi, J., Shen, X., Zhang, S., Liu, Q., 2023b. Small lidar ratio of dust aerosol observed by raman-polarization lidar near desert sources. Opt. Express 31, 16909. https://doi.org/10.1364/OE.484501.

Huang, Z., Shen, X., Tang, S., Zhou, T., Dong, Q., Zhang, S., Li, M., Wang, Y., 2023c. Simulated depolarization ratios for dust and smoke at laser wavelengths: implications for lidar application. Opt. Express 31, 10541. https://doi.org/10.1364/OE.484335.

Indoitu, R., Kozhoridze, G., Batyrbaeva, M., Vitkovskaya, I., Orlovsky, N., Blumberg, D., Orlovsky, L., 2015. Dust emission and environmental changes in the dried bottom of the Aral Sea. Aeolian Res 17, 101–115. https://doi.org/10.1016/j.aeolia.2015.02.004.

Indoitu, R., Orlovsky, L., Orlovsky, N., 2012. Dust storms in Central Asia: spatial and temporal variations. J. Arid Environ. 85, 62–70. https://doi.org/10.1016/j.jaridenv.2012.03.018.

Kim, S.-W., Yoon, S.-C., Kim, J., Kang, J.-Y., Sugimoto, N., 2010. Asian dust event observed in Seoul, Korea, during 29–31 may 2008: analysis of transport and vertical distribution of dust particles from lidar and surface measurements. Sci. Total Environ. 408, 1707–1718. https://doi.org/10.1016/j.scitotenv.2009.12.018.

Li, Zhengpeng, Huang, Z., Bi, J., Dong, Q., Wang, Y., Abdullaev, S.F., Nozirov, D., Li, W., Li, Ze, Meng, Z., Liu, W., Song, X., 2025. Radiative forcing and vertical heating rate of dust aerosols in Southwestern Tajikistan during summer 2023. Atmos. Environ. 345, 121051. https://doi.org/10.1016/j.atmosenv.2025.121051.

Liu, J., Ding, J., Li, X., Zhang, J., Liu, B., 2023. Identification of dust aerosols, their sources, and the effect of soil moisture in central Asia. Sci. Total Environ. 868, 161575. https://doi.org/10.1016/j.scitotenv.2023.161575.

Liu, Q., Huang, Z., Hu, Z., Dong, Q., Li, S., 2022. Long-range transport and evolution of Saharan dust over east Asia from 2007 to 2020. J. Geophys. Res. Atmos. 127. https://doi.org/10.1029/2022JD036974.

Liu, Q., Huang, Z., Liu, J., Chen, W., Dong, Q., Wu, S., Dai, G., Li, M., Li, W., Li, Z., Song, X., Xie, Y., 2024. Validation of initial observation from the first spaceborne high-spectral-resolution lidar with a ground-based lidar network. Atmos. Meas. Tech. 17, 1403–1417. https://doi.org/10.5194/amt-17-1403-2024.

Ma, J., Bi, J., Li, B., Zhu, D., Wang, X., Meng, Z., Shi, J., 2024. Aerosol vertical structure and optical properties during two dust and haze episodes in a typical Valley Basin city, lanzhou of northwest China. Remote Sens. 16, 929. https://doi.org/10.3390/rs16050929.

Ningombam, S.S., Larson, E.J.L., Dumka, U.C., Estellés, V., Campanelli, M., Steve, C., 2019. Long-term (1995–2018) aerosol optical depth derived using ground based AERONET and SKYNET measurements from aerosol aged-background sites. Atmos. Pollut. Res. 10, 608–620. https://doi.org/10.1016/j.apr.2018.10.008.

Papagiannis, S., Abdullaev, S.F., Vasilatou, V., Manousakas, M.I., Eleftheriadis, K., Diapouli, E., 2024. Air quality challenges in Central Asian urban areas: a PM2.5 source apportionment analysis in Dushanbe, Tajikistan. Environ. Sci. Pollut. R. 31, 39588–39601. https://doi.org/10.1007/s11356-024-33833-6.

Perrone, M.R., Lorusso, A., Romano, S., Giles, D.M., Sinyuk, A., Sorokin, M.G., Schafer, J. S., Smirnov, A., Slutsker, I., Eck, T.F., Holben, B.N., Lewis, J.R., Campbell, J.R., Welton, E.J., Korkin, S.V., Lyapustin, A.I., 2022. Advancements in the aerosol robotic network (AERONET) version 3 database – automated near-real-time quality control algorithm with improved cloud screening for sun photometer aerosol optical depth (AOD) measurements. Atmos. Meas. Tech. 12, 169–209. https://doi.org/10.5194/amt-12-169-2019.

Rahnama, M., Attarchi, S., Kashani, S., Baklanov, A., Nickovic, S., Dündar, C., Sealy, A., Tong, D., 2022. WMO Airborne Dust Bulletin, No. 6: Sand and Dust Storm Warning Advisory and Assessment System.

Ramanathan, V., Crutzen, P.J., Kiehl, J.T., Rosenfeld, D., 2001. Aerosols, climate, and the hydrological cycle. Science 294, 2119–2124. https://doi.org/10.1126/science.1064034.

Ren, Y., Yu, H., Liu, C., He, Y., Huang, J., Zhang, L., Hu, H., Zhang, Q., Chen, S., Liu, X., Zhang, M., Wei, Y., Yan, Y., Fan, W., Zhou, J., 2022. Attribution of dry and wet climatic changes over central Asia. J. Clim. 35, 1399–1421. https://doi.org/10.1175/JCLI-D-21-0329.1.

Rupakheti, D., Rupakheti, M., Abdullaev, S.F., Yin, X., Kang, S., 2020a. Columnar aerosol properties and radiative effects over Dushanbe, Tajikistan in central Asia. Environ. Pollut. 265, 114872. https://doi.org/10.1016/j.envpol.2020.114872.

Rupakheti, D., Rupakheti, M., Abdullaev, S.F., Yin, X., Kang, S., 2020b. Columnar aerosol properties and radiative effects over Dushanbe, Tajikistan in central Asia. Environ. Pollut. 265, 114872. https://doi.org/10.1016/j.envpol.2020.114872.

Rupakheti, D., Rupakheti, M., Rai, M., Yu, X., Yin, X., Kang, S., Orozaliev, M.D., Sinyakov, V.P., Abdullaev, S.F., Sulaymon, I.D., Hu, J., 2023. Characterization of columnar aerosol over a background site in central Asia. Environ. Pollut. 316, 120501. https://doi.org/10.1016/j.envpol.2022.120501.

Schuster, G.L., Dubovik, O., Holben, B.N., 2006. Angstrom exponent and bimodal aerosol size distributions. J. Geophys. Res. 111. https://doi.org/10.1029/2005JD006328.

Shao, Y., Wyrwoll, K.-H., Chappell, A., Huang, J., Lin, Z., McTainsh, G.H., Mikami, M., Tanaka, T.Y., Wang, X., Yoon, S., 2011. Dust cycle: an emerging core theme in Earth system science. Aeolian Res 2, 181–204. https://doi.org/10.1016/j.aeolia.2011.02.001.

Shi, L., Zhang, J., Yao, F., Zhang, D., Guo, H., 2020. Temporal variation of dust emissions in dust sources over central Asia in recent decades and the climate linkages. Atmos. Environ. 222, 117176. https://doi.org/10.1016/j.atmosenv.2019.117176.

Shimizu, A., Sugimoto, N., Matsui, I., Arao, K., Uno, I., Murayama, T., Kagawa, N., Aoki, K., Uchiyama, A., Yamazaki, A., 2004. Continuous observations of Asian dust and other aerosols by polarization lidars in China and Japan during ACE-Asia. J. Geophys. Res. Atmos. 109. https://doi.org/10.1029/2002JD003253.

Stein, A.F., Draxler, R.R., Rolph, G.D., Stunder, B.J.B., Cohen, M.D., Ngan, F., 2015. NOAA's HYSPLIT atmospheric transport and dispersion modeling system. Bull. Am. Meteorol. Soc. 96, 2059–2077. https://doi.org/10.1175/BAMS-D-14-00110.1.

Sugimoto, N., Huang, Z., Nishizawa, T., Matsui, I., Tatarov, B., 2012. Fluorescence from atmospheric aerosols observed with a multi-channel lidar spectrometer. Opt. Express 20, 20800. https://doi.org/10.1364/oe.20.020800.

Tao, M., Chen, L., Wang, J., Wang, Lili, Wang, W., Lin, C., Gui, L., Wang, Lunche, Yu, C., Wang, Y., 2022. Characterization of dust activation and their prevailing transport over east Asia based on multi-satellite observations. Atmos. Res. 265, 105886. https://doi.org/10.1016/j.atmosres.2021.105886.

Tegen, I., Lacis, A.A., Fung, I., 1996. The influence on climate forcing of mineral aerosols from disturbed soils. Nature 380, 419–422. https://doi.org/10.1038/380419a0.

Toll, V., Christensen, M., Quaas, J., Bellouin, N., 2019. Weak average liquid-cloud-water response to anthropogenic aerosols. Nature 572, 51–55. https://doi.org/10.1038/s41586-019-1423-9.

Wang, C., Wang, T., Han, Y., Dong, Y., He, S., Tang, J., 2023. Summer extreme dust activity in the taklimakan desert regulated by the South Asian high. Remote Sens. 15, 2875. https://doi.org/10.3390/rs15112875.

Wang, T., Han, Y., Hua, W., Tang, J., Huang, J., Zhou, T., Huang, Z., Bi, J., Xie, H., 2021. Profiling dust mass concentration in northwest China using a joint lidar and sun-photometer setting. Remote Sens. 13. https://doi.org/10.3390/rs13061099.

World Meteorological Organization (WMO), 2024. WMO Airborne Dust Bulletin (WMO No. 8). WMO, Geneva.

Yin, Z., Yi, F., Liu, F., He, Y., Zhang, Yunpeng, Yu, C., Zhang, Yunfei, 2021. Long-term variations of aerosol optical properties over wuhan with polarization lidar. Atmos. Environ. 259, 118508. https://doi.org/10.1016/j.atmosenv.2021.118508.

Zhang, S., Huang, Z., Alam, K., Li, M., Dong, Q., Wang, Y., Shen, X., Bi, J., Zhang, J., Li, W., Li, Z., Wang, W., Cui, Z., Song, X., 2023. Derived profiles of CCN and INP number concentrations in the taklimakan desert via combined polarization lidar, sun-photometer, and radiosonde observations. Remote Sens. 15, 1216. https://doi.org/10.3390/rs15051216.

Zhang, S., Huang, Z., Li, M., Shen, X., Wang, Y., Dong, Q., Bi, J., Zhang, J., Li, W., Li, Z., Song, X., 2022. Vertical structure of dust aerosols observed by a ground-based raman

lidar with polarization capabilities in the center of the taklimakan desert. Remote Sens. 14, 2461. https://doi.org/10.3390/rs14102461.
Zhou, C., Gui, H., Hu, J., Ke, H., Wang, Y., Zhang, X., 2019. Detection of new dust sources in central/east Asia and their impact on simulations of a severe sand and dust storm. J. Geophys. Res. Atmos. 124, 10232–10247. https://doi.org/10.1029/2019JD030753.
Zhou, T., Xie, H., Bi, J., Huang, Z., Huang, J., Shi, J., Zhang, B., Zhang, W., 2018. Lidar measurements of dust aerosols during three field campaigns in 2010, 2011 and 2012 over northwestern China. Atmosphere 9. https://doi.org/10.3390/atmos9050173.
Zhou, T., Xie, H., Jiang, T., Huang, J., Bi, J., Huang, Z., Shi, J., 2021. Seasonal characteristics of aerosol vertical structure and autumn enhancement of non-spherical particle over the semi-arid region of northwest China. Atmos. Environ. 244, 117912. https://doi.org/10.1016/j.atmosenv.2020.117912.
Zhou, T., Zhou, X., Yang, Z., Córdoba-Jabonero, C., Wang, Y., Huang, Z., Da, P., Luo, Q., Zhang, Z., Shi, J., Bi, J., Alikhodja, H., 2024. Transboundary transport of non-east and East Asian dust observed at dunhuang, northwest China. Atmos. Environ. 318, 120197. https://doi.org/10.1016/j.atmosenv.2023.120197.
Zhou, X., Zhou, T., Fang, S., Han, B., He, Q., 2023. Investigation of the vertical distribution characteristics and microphysical properties of summer mineral dust masses over the taklimakan desert using an unmanned aerial vehicle. Remote Sens. 15, 3556. https://doi.org/10.3390/rs15143556.
Zhu, C., Cao, J., Hu, T., Shen, Z., Tie, X., Huang, H., Wang, Q., Huang, R., Zhao, Z., Močnik, G., Hansen, A.D.A., 2017. Spectral dependence of aerosol light absorption at an urban and a remote site over the Tibetan Plateau. Sci. Total Environ. 590–591, 14–21. https://doi.org/10.1016/j.scitotenv.2017.03.057.